Brittle-ductile behavior of a nanocrack in nanocrystalline Ni: A quasicontinuum study*

Shao Yu-Fei(邵宇飞)[a], Yang Xin(杨 鑫)[a], Zhao Xing(赵 星)[b]†, and Wang Shao-Qing(王绍青)[c]

[a] *Institute of Applied Physics and Technology, Department of General Studies, Liaoning Technical University, Huludao* 125105, *China*

[b] *Department of Mathematics and Physics, Liaoning University of Technology, Jinzhou* 121001, *China*

[c] *Shenyang National Laboratory for Materials Science, Institute of Metal Research, Chinese Academy of Sciences, Shenyang* 110016, *China*

(Received 23 December 2011; revised manuscript received 12 March 2012)

The effects of stacking fault energy, unstable stacking fault energy and unstable twinning fault energy on the fracture behavior of nanocrystalline Ni are studied via the quasicontinuum simulations. Two semi-empirical potentials for Ni are used to vary the values of these generalized planar fault energies. When the above three energies are reduced, a brittle-to-ductile transition of the fracture behavior is observed. In the model with higher generalized planar fault energies, a nanocrack proceeds along a grain boundary, while in the model with lower energies, the tip of the nanocrack becomes blunt. A greater twinning tendency is also observed in the more ductile model. These results indicate that the fracture toughness of nanocrystalline face-centered-cubic metals and alloys might be efficiently improved by controlling the generalized planar fault energies.

Keywords: atomistic simulations, nanocrystalline materials, fracture, grain boundaries

PACS: 31.15.xv, 61.72.Mm, 62.20.mt, 61.82.Rx **DOI:** 10.1088/1674-1056/21/9/093104

1. Introduction

In the past decades, much attention has been paid to materials on nanoscale, such as nanoparticles and nanocrystalline (NC) metals.[1−6] NC materials usually have high strength, but very low ductility.[1,2,7] Many strategies have been applied to increasing the ductility.[8] Unfortunately, most of them result in a decrease in strength. Recently, twins and stacking faults generated by Shockley partials in NC face-centered-cubic (fcc) metals have been studied intensively.[9−13] It has been reported that both the strength and the ductility of NC fcc metals can benefit from twins. Hence, promoting the tendency of twinning seems to be one of the most promising methods for simultaneously improving the strength and ductility.[14] Most recently, experimental investigations indicate that a reduction in stacking fault energy ($\gamma_{\rm sf}$) may enhance the activity of deformation twins, and thus improve the ductility of NC fcc metals and alloy.[15−17] However, the formation of a deformation twin is dominated not only by stacking fault energy, but also by unstable stacking fault energy ($\gamma_{\rm usf}$) and unstable twinning fault energy ($\gamma_{\rm utf}$).[18,19] As depicted in Fig. 1, these three kinds of planar fault energies are the extrema of the generalized planar fault energy (GPFE) curve which represents the energy cost of shifting two semi-infinite blocks of fcc crystal on {111} planes along the ⟨112⟩ direction.[18,20] Starting from a perfect fcc structure, the lattice will have to pass through the unstable stacking fault energy barrier to nucleate a partial dislocation. After the partial dislocation begins to slip, an intrinsic stacking fault ribbon associated with the energy cost $\gamma_{\rm sf}$ will be left behind. Starting from the lattice configuration with a pre-existing intrinsic stacking fault defect, the unstable twinning fault energy has to be overcome, so that a partial dislocation with the same burgers vector can propagate on the adjacent slipping plane. After the twinning partial dislocation starts to slip, an extrinsic stacking fault defect or, equivalently, a micro-twin will be created. Usually, the two energy barriers ($\gamma_{\rm usf}$ and $\gamma_{\rm utf}$) cannot be measured by experiments. Thus, how the reductions in these three generalized planar fault energies influence the mechanical behavior of NC fcc metals and alloys is still unclear.

*Project supported by the National Basic Research Program of China (Grant No. 2011CB606403).

†Corresponding author. E-mail: yfshao@alum.imr.ac.cn; zhao-heng-xing@126.com

© 2012 Chinese Physical Society and IOP Publishing Ltd

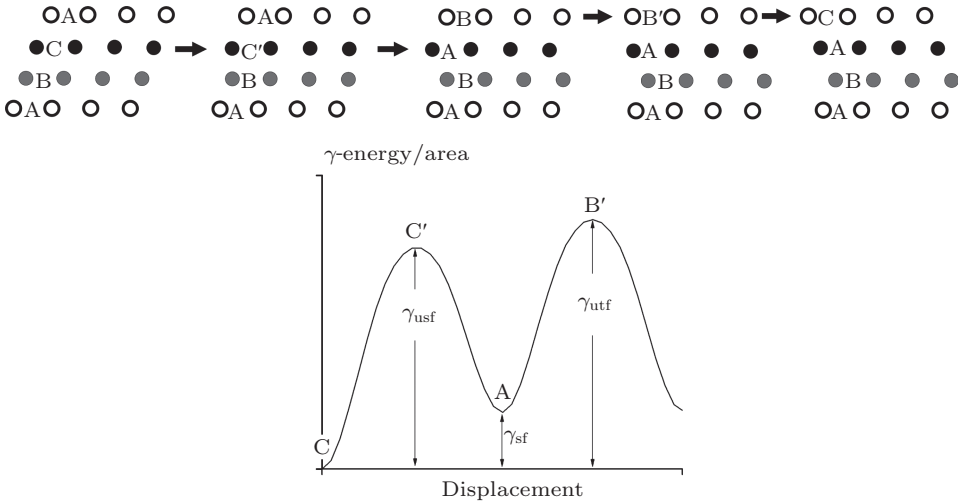


Fig. 1. Schematic representation of GPFE curve for an fcc metal. The stacking sequence of {111} planes in the lattice is ABCABCA... After a partial dislocation propagates along the ⟨112⟩ direction, half of the crystal will be shifted. The slipped {111} planes will be changed by the following sequence: C→A→B→C. C′ and B′ indicate the lattice configurations corresponding to the unstable stacking fault energy barrier and the unstable twinning fault energy barrier respectively.

This work is to study the effect of the three planar fault energies $\gamma_{\rm sf}$, $\gamma_{\rm usf}$, and $\gamma_{\rm utf}$ on the ductility of NC fcc metals by computational simulations. A novel multiscale method, i.e., the quasicontinuum (QC) method, is adopted.[21,22] The QC method can be used to study local physical phenomena in models spanning several length scales and obtain the same results as classical atomistic simulations with a fraction of the computational cost.[23–26] Nickel is chosen as a trial material in this work, because of its wide application. With the reductions of $\gamma_{\rm sf}$, $\gamma_{\rm usf}$, and $\gamma_{\rm utf}$, it is found that the ductility of NC Ni can be efficiently improved. To address the issue of ductility improvement, variations of structure and stress on atomic level are also analyzed.

2. Methodology

2.1. QC simulations

The QC method used here is a mixture of continuum and lattice statics method. The basic principle of QC is that discrete defects in a crystal are explicitly studied on the atomic level, while the majority of the crystal is approximately treated as finite elements. The energies of atoms in the QC model can be calculated by empirical potentials, such as the embedded-atom-method.[27] The equilibrium configuration of the system can be established through minimization of the total energy respect to atomic positions. More details of the QC method can be found in the review article written by Miller and Tadmor.[28]

The QC model for NC Ni is presented in Fig. 2. Same as our previous work,[24] there was a pre-existing crack in the block. This block was 400 nm×400 nm in the x–y plane, and periodically repeated in the z direction. The width and length of the crack were approximately 2.5 nm and 194 nm respectively. The crack tip was surrounded by a full atomic zone which is framed by dark lines. As illustrated in Fig. 2(b), the size of the atomic zone was 36 nm×36 nm. The averaged grain size was 5 nm. The grains in the atomic zone were constructed based on the Voronoi diagram,[29] and each grain had a common [−110] out-of-plane direction and a random in-plane orientation. Two grains in front of the crack tips were labeled as 1 and 2. For simplicity, the grain boundary (GB) between the grains 1 and 2 was termed as GB 1–2. The region out of the atomic zone was filled by a single crystal and coarsened by finite element meshes.

The QC samples were in the opening loading condition. According to the anisotropic linear elastic fracture mechanics (LEFM),[30] displacements of all atoms are calculated as follows:

$$u(X) = u(X) + u_{\rm LEFM}(X, \Delta K), \qquad (1)$$

where u is the displacement field, X is the position of any atom in the model, $u_{\rm LEFM}$ is the anisotropic LEFM solution, and ΔK is the increment of stress intensity factor K. In the present simulation, K starts

from zero and ΔK is 0.008 MN·m$^{-3/2}$. The displacements of atoms at boundaries (except the crack faces) were kept fixed, while the positions of all other atoms could be adjusted by energy relaxation. During the relaxation process, the total energy was minimized until the sum of out-of-balance forces over the entire system was less than 1.602 μN.

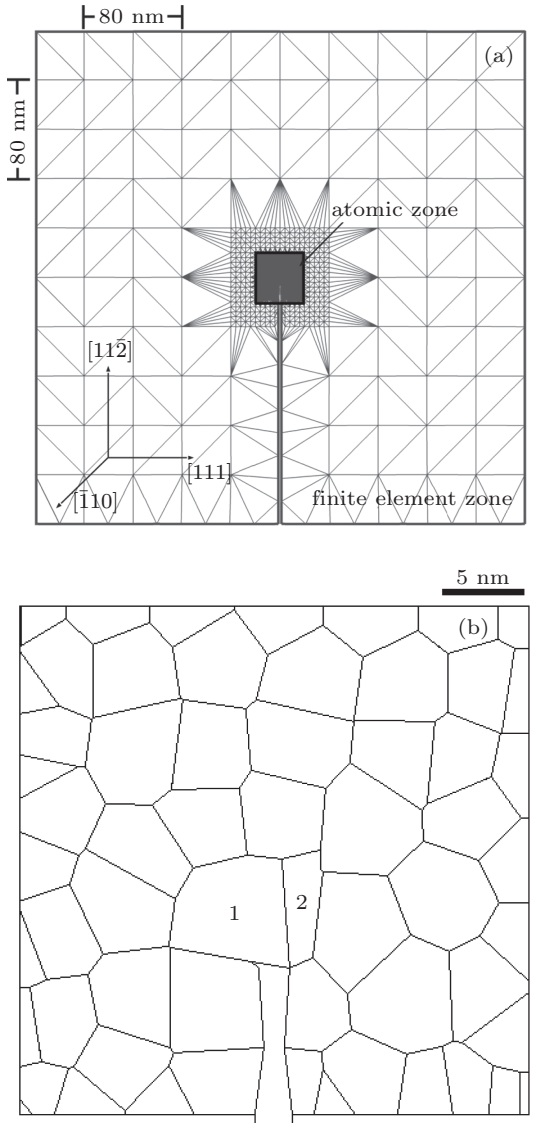


Fig. 2. The QC model for NC Ni with a pre-existing crack: (a) full size view of both finite element and atomic zones, (b) grain structure of atomic zone.

The visualizing software "Atomeye"[31] combined with the common neighbor analysis method[32] was used to display the atomic configurations of QC results. The atomic local stress states within QC samples were calculated as follows:[33]

$$\sigma_i^{\alpha\beta} = \frac{1}{\Omega}\left\{\frac{p_l^\alpha p_l^\beta}{m_l}\Lambda_l + \frac{1}{2}\sum_{k\neq l}\left(-\frac{\partial\varphi}{\partial r}\right)\frac{r^\alpha r^\beta}{r}\eta_{lk}(r)\,|_{r=r_{lk}}\right\}, \quad (2)$$

where Ω, called averaging volume, is the spherical volume centered on the i-th atom with a specific radius, α and β are the Cartesian coordinates, P_l and m_l are the momentum and mass of the l-th atom, Λ_l is unity if the atom l lies within the averaging volume and is zero otherwise, φ is the interatomic potential, r_{lk} is the distance between the l-th and k-th atoms, and $\eta_{lk} = \eta_{kl}$ is the fractional length of the l–k bond that lies within the averaging volume Ω. In this work, the radius of Ω is taken as 0.5 nm in all the simulations. Since the QC model is quasi-static, only the second part in the braces is considered.

2.2. GPFE curves obtained by the quasicontinuum method

To study the effect of reductions in the three planar fault energies $\gamma_{\rm sf}$, $\gamma_{\rm usf}$, and $\gamma_{\rm utf}$, two different embedded-atom-method potentials for Ni were used, which are the potentials developed by Voter and Chen

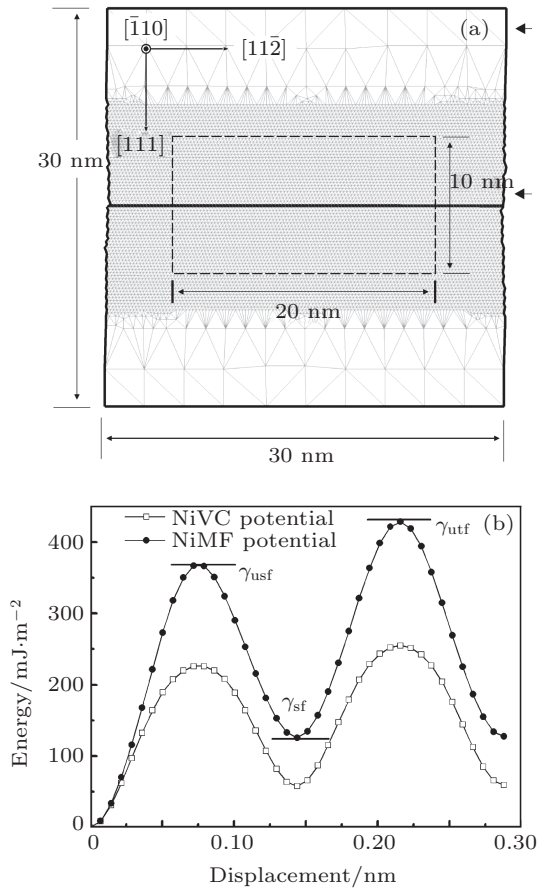


Fig. 3. GPFE calculation of Ni: (a) the QC model for a single crystal Ni, (b) GPFE curves obtained by the QC method with the NiMF and NiVC potentials.

(NiVC potential)[34] and the potential proposed by Mishin *et al.* (NiMF potential).[35] A single crystal simulated by the QC method is presented in Fig. 3(a). Starting from a perfect fcc structure, the upper half of the block was rigidly sheared with respect to the lower half in a small increment along the $[-1\ -\ 12]$ direction. Except the atoms belonging to the top and bottom boundaries, all atoms in the digital sample are allowed to relax along the $[-110]$ and the $[111]$ directions after each loading step. By summing up the energies of atoms in the dashed region, the average energy per unit area of the slip plane is calculated and plotted in Fig. 3(b). Clearly, the values of $\gamma_{\rm sf}$, $\gamma_{\rm usf}$, and $\gamma_{\rm utf}$ predicted by NiVC potential are much lower than the ones predicted by NiMF potential.

3. Results

3.1. Morphologies of crack tip

The morphologies of the nanocrack tip described by the NiMF and NiVC potentials are displayed in Fig. 4. When K is 0.897 MN·m$^{-3/2}$, there are only a few slight differences between the structures of the models, because of the different potential functions. However, when K is increased to 0.905 MN·m$^{-3/2}$, many different features are observed in the two models. The model described by the NiMF potential presents a brittle behavior, since the crack tip proceeds along the GB 1–2. A ductile feature appears in the model described by the NiVC potential, since the crack tip becomes blunt.

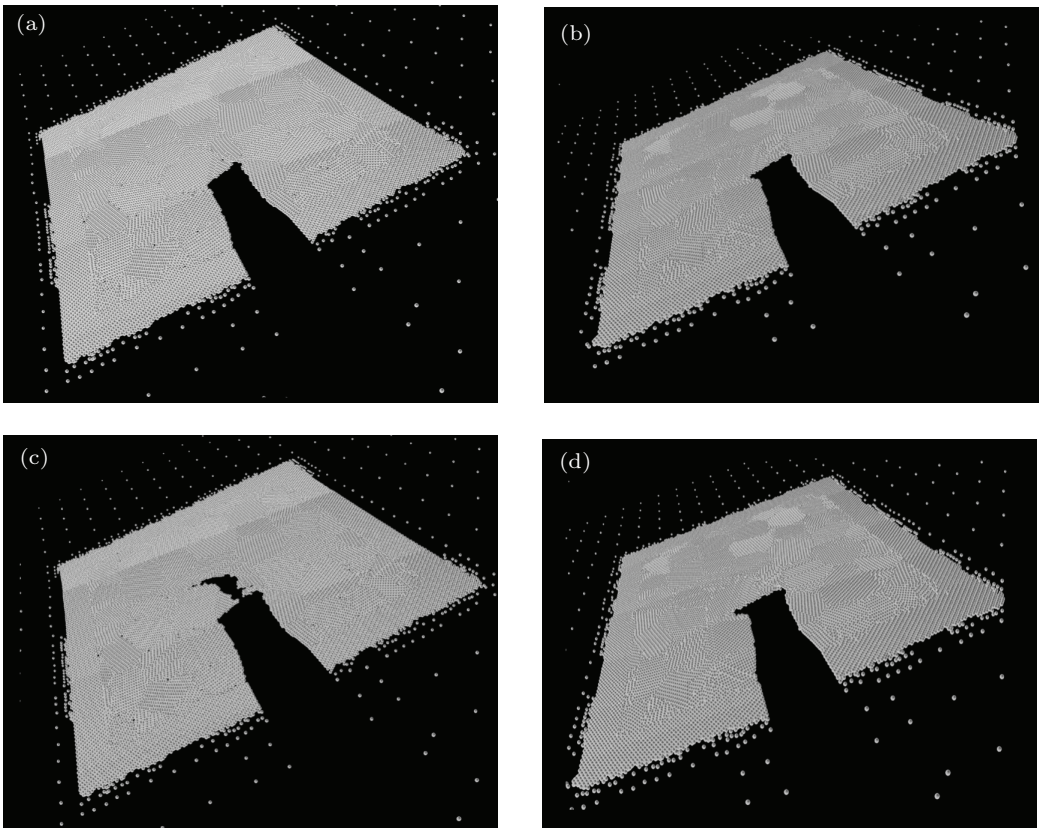


Fig. 4. Morphologies of crack tip at different values of stress intensity factor K: (a) the NiMF model, K = 0.897 MN·m$^{-3/2}$; (b) the NiVC model, K = 0.897 MN·m$^{-3/2}$; (c) the NiMF model, K = 0.905 MN·m$^{-3/2}$; (d) the NiVC model, K = 0.905 MN·m$^{-3/2}$.

3.2. Hydrostatic stress distributions in the regions ahead of crack tip

In Fig. 5, the hydrostatic stress distributions in the regions ahead of crack tips in the NiMF and NiVC models are illustrated. Clearly, the region of the GB 1–2 ahead of the crack tip in the NiMF model is undergoing a high tensile hydrostatic stress state before the crack begins to propagate. After the propagation process, the atomic tensile stresses are greatly released. In the NiVC model, the hydrostatic stress states experienced by the GB 1–2 during the loading steps are much milder.

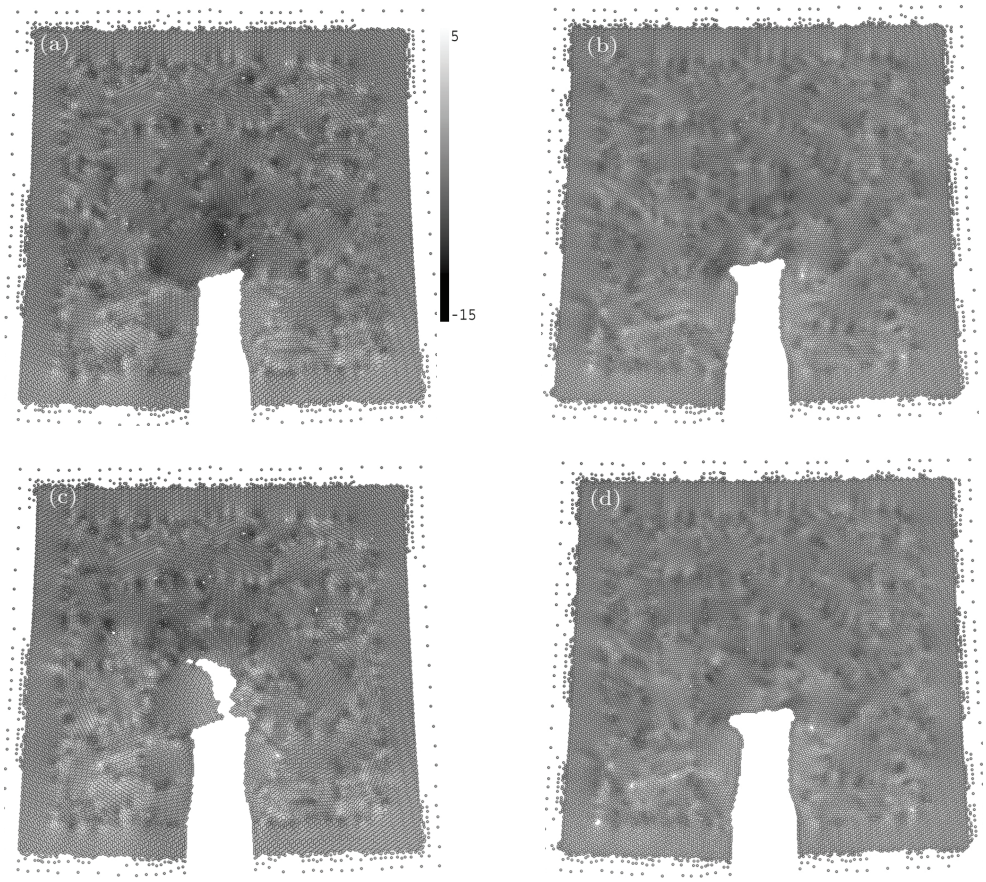


Fig. 5. (colour online) Hydrostatic stress distributions in the region ahead of crack tip. The unit of stress is GPa. (a) The NiMF model, $K = 0.897$ MN·m$^{-3/2}$; (b) the NiVC model, $K = 0.897$ MN·m$^{-3/2}$; (c) the NiMF model, $K = 0.905$ MN·m$^{-3/2}$; (d) the NiVC model, $K = 0.905$ MN·m$^{-3/2}$.

3.3. Defects in the regions ahead of crack tip

Both computational[36] and experimental[37] results indicate that dislocation activities can exist in the regions near the crack tip in NC Ni. In this work, both stacking faults and deformation twins are observed in the regions around the crack tips in the two models when K reaches 0.897 MN·m$^{-3/2}$. Distributions of stacking faults and deformation twins are presented in Fig. 6. There are more stacking faults and deformation twins in the NiVC model than in the NiMF model on the same loading level. This indicates an enhanced dislocation activity in the NiVC model.

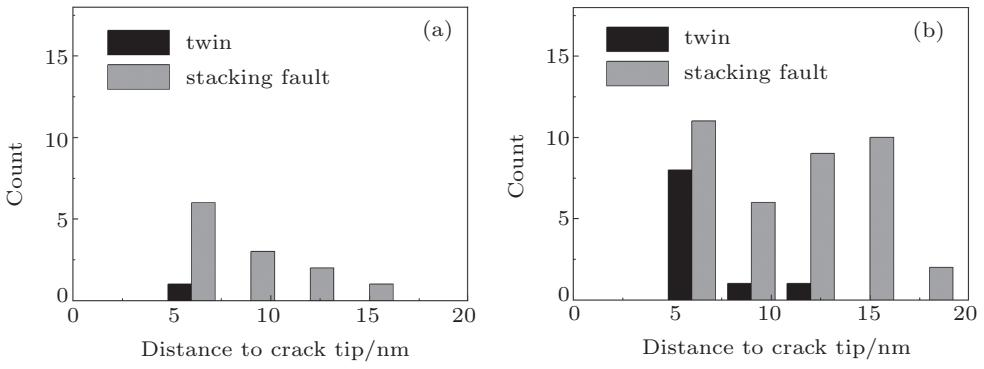


Fig. 6. (colour online) Statistics of deformation twin and stacking fault in the region around the crack tip when $K = 0.897$ MN·m$^{-3/2}$: (a) the NiMF model, (b) the NiVC model.

3.4. Atomic structures of the GB 1–2

In Fig. 7, atomic structures of the grains 1 and 2 in the two models are shown. White, gray and black atoms are in local fcc, hexagonal-close-packed (hcp) and defect structures respectively. One layer of hcp atoms is identified as a coherent twin boundary. Two consecutive layers of hcp atoms indicate a stacking fault. In Figs. 7(a) and 7(b), there are some slight differences for the initial relaxed atomic structures of the GB 1–2, due to the differences between potential functions used in the two models. From Figs. 7(c) and 7(d), when K reaches 0.905 MN·m$^{-3/2}$, only one twin boundary is nucleated in grain 1 and the GB 1–2 is cleaved in the NiMF model; while in the NiVC model, several stacking faults are found in grain 1 and the GB 1–2 is still in a stable state. Hence, the fracture behavior of NC Ni is transformed from brittle features to ductile features, because of the promoted dislocation activity in the grains around crack tip.

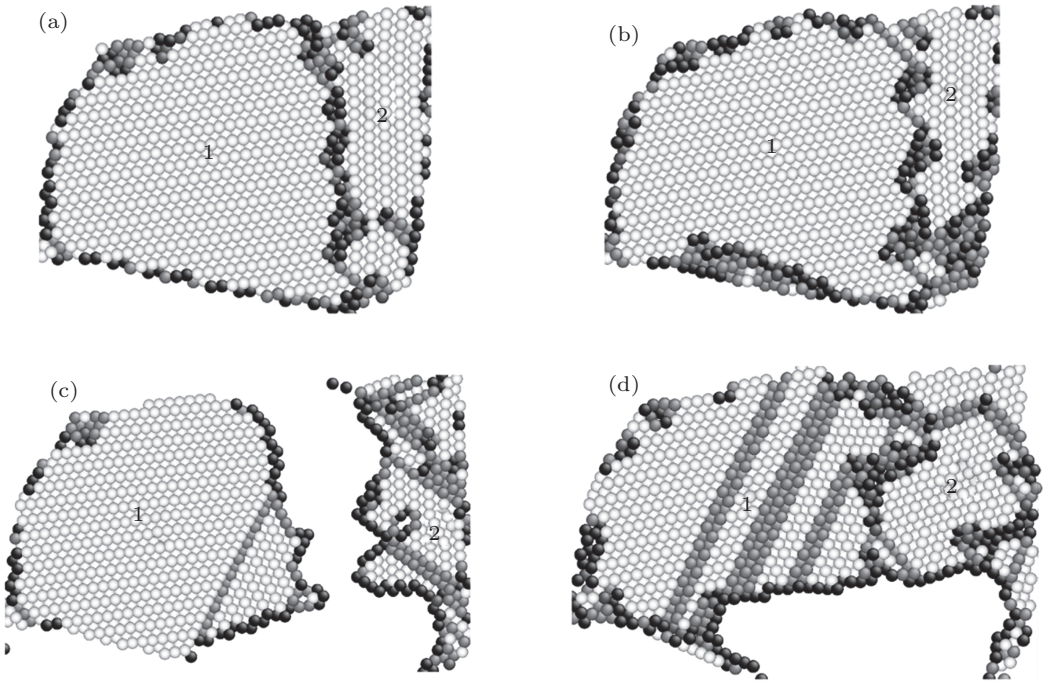


Fig. 7. Relaxed atomic structures of the GB 1–2: (a) the NiMF model, before loading; (b) the NiVC model, before loading; (c) the NiMF model, $K = 0.905$ MN·m$^{-3/2}$; (d) the NiVC model, $K = 0.905$ MN·m$^{-3/2}$.

4. Discussion

The three generalized planar fault energies, $\gamma_{\rm sf}$, $\gamma_{\rm usf}$, and $\gamma_{\rm utf}$, have been focused for years. In 1926, a simple sinusoidal function to express the energy per unit area for the two atomic layers sheared from their equilibrium arrangement was proposed by Frenkel.[38] Later, Mackenzie suggested a more complex sinusoidal function to the slip of {111} planes in an fcc crystal.[39] In 1992, Rice labeled the maximum of the energy-displacement curve developed by Frenkel and Mackenzie as the unstable stacking fault energy, $\gamma_{\rm usf}$.[40] Recently, the unstable twinning fault energy, $\gamma_{\rm utf}$, was introduced by Tadmor and Hai.[12,41] Later, a material parameter for measuring twinnability of fcc metals and alloys, $\tau_{\rm a} = \left[1.136 - 0.151\dfrac{\gamma_{\rm sf}}{\gamma_{\rm usf}}\right]\sqrt{\dfrac{\gamma_{\rm usf}}{\gamma_{\rm utf}}}$, was defined by Bernstein and Tadmor.[42] A larger $\tau_{\rm a}$ indicates a greater tendency for twinning. Based on this newly proposed twinning parameter, some Ni alloys were studied by the density functional theory calculations.[43] In the present simulations, according to the GPFE curves in Fig. 3(b), the value of $\tau_{\rm a}$ derived from NiVC potential is about 1.033, while $\tau_{\rm a} \approx 1.004$ for the NiMF potential. Thus, compared with the NiMF model, the NiVC model exhibits an enhanced twinning ability. This theoretical prediction is verified by the statistics of defects illustrated in Fig. 6.

Although the positive effect of twin boundaries in NC Ni on the fracture toughness has been clarified by Zhou *et al.*,[44] the ductility improvement of Ni in our simulations is due to the enhanced dislocation activity, not the presence of deformation twins. How

the deformation twins in the grains ahead of crack tip influence the behavior of the nanocrack is not investigated in this work, because of the limited computational resources. In the present NiVC model, the energy barrier for nucleating a partial dislocation is lowered by the reduction of the unstable stacking fault energy $\gamma_{\rm usf}$. Hence, the dislocation activity in the regions ahead of crack tip is promoted, accompanied by release of the atomic tensile hydrostatic stresses. Meanwhile, the atomic configuration of the crack tip is modified to be blunt by emitting partial dislocations.

It should be emphasized that the fracture behavior of metals might be influenced by many factors, such as environmental temperature,[45] impurities,[46] initial configuration of crack tip,[12] crystal orientation,[47] and distribution of internal boundaries.[48] In the present work, the initial geometrical configuration of the crack tip is constructed randomly, and only the fracture behavior of NC Ni at low temperature is studied. The research on NC Ni at high temperature is beyond the QC simulations, since the QC method is based on lattice statics. In addition, the QC models in the present simulations are simplified by the digital samples composed of small grains without impurities. In the future work, some necessary material parameters will be considered. Even so, some meaningful results are still obtained in the present work. Controlling the generalized planar fault energies might be an efficient way to improve the fracture toughness of NC fcc metals and alloys.

5. Conclusions

In summary, the effects of the three kinds of planar fault energies, i.e., the stacking fault energy $\gamma_{\rm sf}$, the unstable stacking fault energy $\gamma_{\rm usf}$, and the unstable twinning fault energy $\gamma_{\rm utf}$, on the fracture behavior of NC Ni are studied via the QC simulations. Models spanning several length scales with two semi-empirical potentials for Ni are adopted. A nanocrack in the NC Ni proceeds along a GB, when the digital sample is loaded to a certain level. Once the three planar fault energies are reduced, the mechanical behavior of the nanocrack is transformed from the brittle features to the ductile features. A greater twinning tendency is also observed in the more "ductile" model. These results suggest that the fracture toughness of NC fcc metals and alloys might be efficiently improved by controlling the generalized planar fault energies.

Acknowledgements

The authors would like to thank Tadmor and Miller for their quasicontinuum code and Sloan for his constrained Delaunay triangulating code. The first author appreciates the helpful discussion with Mr. Wan in IMR, CAS, and Dr. Dupont in US.

References

[1] Meyers M A, Mishra A and Benson D J 2006 *Prog. Mater. Sci.* **51** 427
[2] Dao M, Lu L, Asaro R J, Hosson J T M and Ma E 2007 *Acta Mater.* **55** 4041
[3] Ma W, Zhu W J, Zhang Y L and Jing F Q 2011 *Acta Phys. Sin.* **60** 066404 (in Chinese)
[4] Shao C W, Wang Z H, Li Y N, Zhao Q and Zhang L 2011 *Acta Phys. Sin.* **60** 083602 (in Chinese)
[5] Song C F, Fan Q N, Li W, Liu Y L and Zhang L 2011 *Acta Phys. Sin.* **60** 063104 (in Chinese)
[6] Wang Z G, Wu L, Zhang Y and Wen Y H 2011 *Acta Phys. Sin.* **60** 096105 (in Chinese)
[7] Ma E 2003 *Scripta Mater.* **49** 663
[8] Ma E 2006 *JOM* **58** 49
[9] Zhu Y T, Narayan J, Hirth J P, Mahajan S, Wu X L and Liao X Z 2009 *Acta Mater.* **57** 3763
[10] Wu X L and Zhu Y T 2008 *Phys. Rev. Lett.* **101** 025503
[11] Lu L 2008 *J. Mater. Sci. Technol.* **24** 473
[12] Hai S and Tadmor E B 2003 *Acta Mater.* **51** 117
[13] Yamakov V, Wolf D, Phillpot S R and Gleiter H 2002 *Acta Mater.* **50** 5005
[14] Lu K, Lu L and Suresh S 2009 *Science* **324** 349
[15] Zhao Y H, Zhu Y T, Liao X Z, Horita Z and Langdon T G 2006 *Appl. Phys. Lett.* **89** 121906
[16] Sun P L, Zhao Y H, Cooley J C, Kassner M E, Horita Z and Langdon T G 2009 *Mater. Sci. Eng.* A **525** 83
[17] Wang Z W, Wang Y B, Liao X Z, Zhao Y H, Lavernia E J, Zhu Y T, Horita Z and Langdon T G 2009 *Scripta Mater.* **60** 52
[18] Swygenhoven H V, Derlet P M and Froseth A G 2004 *Nature Mater.* **3** 399
[19] Jin J, Shevlin S A and Guo Z X 2008 *Acta Mater.* **56** 4358
[20] Zimmerman J A, Gao H J and Abraham F F 2000 *Modeling Simul. Mater. Sci. Eng.* **8** 103
[21] Tadmor E B, Phillips R and Ortiz M 1996 *Langmuir* **12** 4529
[22] Tadmor E B, Ortiz M and Phillips R 1996 *Philos. Mag.* A **73** 1529
[23] Wang H T, Qin Z D, Ni Y S and Zhang W 2009 *Acta Phys. Sin.* **58** 1057 (in Chinese)
[24] Shao Y F and Wang S Q 2010 *Acta Phys. Sin.* **59** 7258 (in Chinese)
[25] Lu H B, Li J W, Ni Y S, Mei J F and Wang H S 2011 *Acta Phys. Sin.* **60** 106101 (in Chinese)
[26] Mei J F, Li J W, Ni Y S and Wang H T 2011 *Acta Phys. Sin.* **60** 066104 (in Chinese)
[27] Daw M S and Baskes M I 1984 *Phys. Rev.* B **29** 6443
[28] Miller R E and Tadmor E B 2002 *J. Computer-Aided Mater. Design* **9** 203

[29] Voronoi G Z 1908 *J. Reine Angew. Math.* **134** 199
[30] Sih G C and Liebowitz H 1968 *Fracture: An Advanced Treatise*, (NewYork: Academic Press) pp. 67–190
[31] Li J 2003 *Modeling Simul. Mater. Sci. Eng.* **11** 173
[32] Honeycutt J D and Andersen H C 1987 *J. Phys. Chem.* **91** 4950
[33] Cormier J, Rickman J M and Delph T J 2001 *J. Appl. Phys.* **89** 99
[34] Voter A F and Chen S P 1987 *Mater. Res. Soc. Symp. Proc.* **82** 175
[35] Mishin Y, Farkas D, Mehl M J and Papaconstantopoulos D A 1999 *Phys. Rev.* B **59** 3393
[36] Farkas D, Petegem S V, Derlet P M and Swygenhoven H V 2005 *Acta Mater.* **53** 3115
[37] Kumar K S, Suresh S, Chisholm M F, Horton J A and Wang P 2003 *Acta Mater.* **51** 387
[38] Frenkel J 1926 *Z. Phys.* **37** 572
[39] Mackenzie J K 1949 *A Theroy of Sintering and the Theoretical Yield Strength of Solids* (PhD Thesis) (Bristol: Bristol University)
[40] Rice J R 1992 *J. Mech. Phys. Solids* **40** 239
[41] Tadmor E B and Hai S 2003 *J. Mech. Phys. Solids* **51** 765
[42] Bernstein N and Tadmor E B 2004 *Phys. Rev.* B **69** 094116
[43] Siegel D J 2005 *Appl. Phys. Lett.* **87** 121901
[44] Zhou H F, Qu S X and Yang W 2010 *Modeling Simul. Mater. Sci. Eng.* **18** 065002
[45] Yamakov V, Saether E and Glaessgen E H 2008 *J. Mater. Sci.* **43** 7488
[46] Kart H H, Uludogan M and Cagin T 2009 *Comput. Mater. Sci.* **44** 1236
[47] Miller R E, Tadmor E B, Phillips R and Ortiz M 1998 *Modeling Simul. Mater. Sci. Eng.* **6** 607
[48] Hasnaoui A, Swygenhoven H V and Derlet P M 2003 *Science* **300** 1550